

## Low-Valency Nitridonickelates

Peter Höhn, Rainer Niewa, Zhong-Le Huang\*, Akash Mehta, Vladimir Ivanshin, Jörg Sichelschmidt, Walter Schnelle, Zhiwei Hu\*\* and Rüdiger Kniep

Inorganic compounds with nickel in the oxidation state +1 are rarely known. In oxide chemistry only few examples are reported [1], all with  $\text{Ni}^{+1}$  in linear coordination by oxo-ligands. In the last decade only, the study of ternary and higher nitridometalates has been a rapidly growing field of inorganic solid state chemistry [2,3] and led to an abundance of  $\text{Ni}^{+1}$  compounds. Ternary lithium nitridonickelates(I)  $\text{Li}_2[(\text{Li}_{1-x}\text{Ni}_x)\text{N}]$  (Fig. 1), derived from the binary fast lithium ion conductor  $\alpha\text{-Li}_3\text{N} \equiv \text{Li}_2[\text{LiN}]$  [4], have attracted considerable attention. The crystal structures of phases  $\text{Li}_2[(\text{Li}_{1-x}\text{M}_x)\text{N}]$  with  $M = \text{Cu}, \text{Ni}, \text{Co}$  have already been reported as early as 1949 by Sachsze and Juza [5]. Recently, the respective substitution phases with  $M = \text{Mn}, \text{Fe}$  were also described [6].

In contrast to the ternary lithium substitution phases, the ternary alkaline earth nitridonickelates  $\text{Ca}[\text{Ni}^{+1}\text{N}]$  [7, 8],  $\text{Sr}[\text{Ni}^{+1}\text{N}]$  [9],  $\text{Ba}[\text{Ni}^{+1}\text{N}]$  [10], and  $\text{Ba}_8\text{N}[\text{Ni}^{+5/6}\text{N}]_6$  [11] show no substitution effects between nickel and the alkaline earth elements. A recent re-investigation of the system Ba-Ni-N resulted in the compound  $\text{Ba}_2[\text{Ni}_3\text{N}_2]$  [12] (Fig. 2a). The distinct and low average oxidation states fueled our interest in the electronic and magnetic properties of these compounds. Also in qua-

ternary lithium alkaline-earth nitridonickelates, substitution of nickel by lithium takes place readily [13], but up to now, no data on physical properties are available.

The crystal structure of  $\alpha\text{-Li}_3\text{N} \equiv \text{Li}_2[\text{LiN}]$  (Fig. 1) contains infinite chains  ${}^1_{\infty}[\text{LiN}_{2/2}]$  of alternating nitrogen and lithium (Li(1)) atoms. These chains are interconnected via further Li(2) in trigonal planar coordination by N within the layers formed by the nitride species (“ $\text{Li}_2\text{N}$ ”-layers) [4]. In the crystal structure of  $\text{Li}_2[(\text{Li}_{1-x}\text{Ni}_x)\text{N}]$ , the linearly by nitrogen coordinated Li(1) site is partially substituted by Ni in a random manner. For the Ni substitution series single phase samples with  $x$  up to 0.85(1) were obtained, while a sample with  $x = 0.93$  contained small amounts of elemental Ni. The samples were of deep maroon color at low  $x$  and brass colored for  $x \geq 0.79$ . This change in color as a function of  $x$  is associated with the appearance of metallic conductivity at high  $x$  values (see below). The dependences of the unit cell parameters  $a$  and  $c$ , of the average chain length  $q = 1 + x/(1-x)$ , and of the distance  $d(\text{Li}/\text{Ni}-\text{N})$  on  $x$  are plotted in Fig. 3. With increasing  $x$  the parameter  $c$  decreases nearly linearly (the data of the  $x = 0.34(1)$  and  $x = 0.43(1)$  samples included in the plot were previously determined on single crystals [13]). In contrast, the parameter  $a$ , related to the distance  $d(\text{Li}(2)-\text{N})$  within the crystallographic (001) plane, increases only slightly. The parameters  $c$  of phases with  $x \geq 0.79$  are already shorter than two times the bond lengths in the structurally related compounds  $\text{Li}[\text{Ni}^{+2}\text{N}]$  [14],  $\text{Li}_5[\text{Ni}^{+1.33}\text{N}]_3$  [14, 15] and  $\text{Ca}[\text{Ni}^{+1}\text{N}]$  [7, 8]. Based on our X-ray diffraction Rietveld refinements, the characteristic mass changes during TG experiments, and the chemical analyses, the vacancy concentration within the basal plane (Li(2)) is much lower ( $\leq 5\%$ ) than concluded from neutron diffraction studies by different authors (17% – 42% [16, 17]). The magnetic moments observed in samples of the isostructural copper series  $\text{Li}_2[(\text{Li}_{1-x}\text{Cu}_x)\text{N}]$  indicate, that the Li(2) vacancy concentration, which is expected to lead to the formation of  $M^{+2}$  species, must be even smaller ( $\leq 1\%$ ).

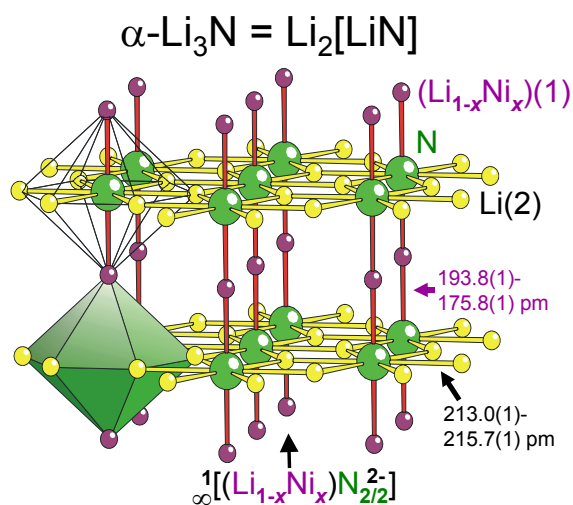


Fig.1: Crystal structure of  $\alpha\text{-Li}_3\text{N} \equiv \text{Li}_2[\text{LiN}]$  and  $\text{Li}_2[(\text{Li}_{1-x}\text{Ni}_x)\text{N}]$ .

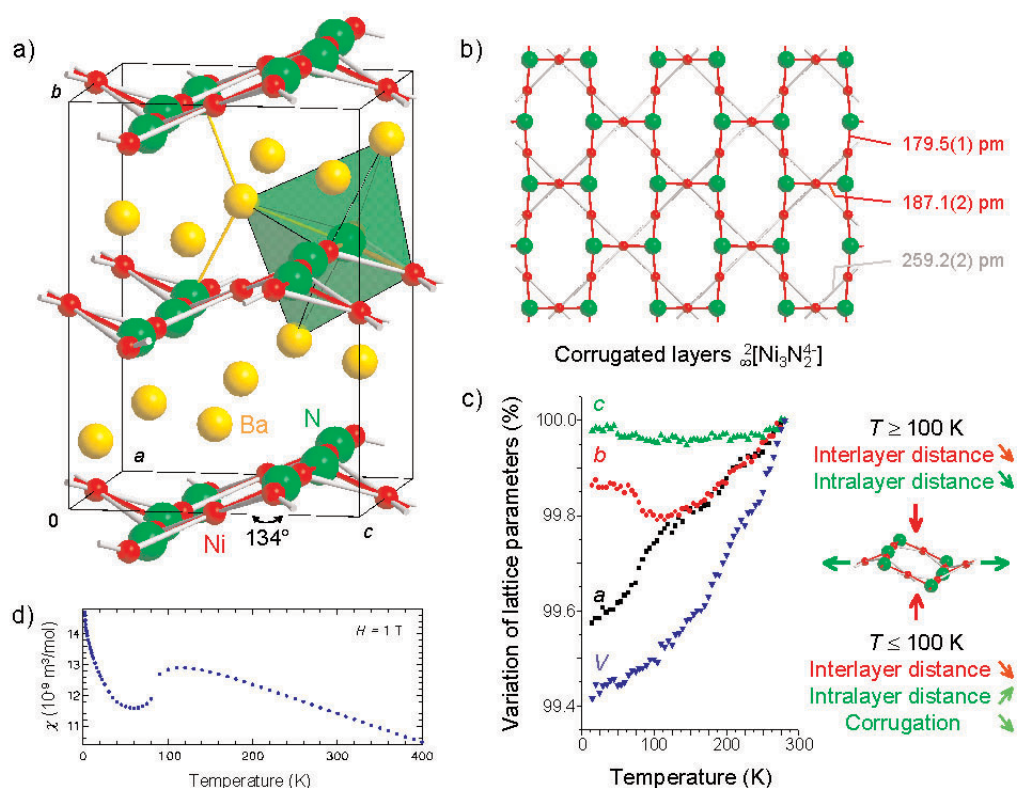


Fig. 2: a) Crystal structure of  $Ba_2[Ni_3N_2]$ , b) The complex anion  ${}^2_3[Ni_3N_2^{4-}]$ , c)  $Ba_2[Ni_3N_2]$ : Lattice parameters as a function of temperature. Presumable structural changes within the complex anion  ${}^2_3[Ni_3N_2^{4-}]$  with decreasing temperature are illustrated, d) Magnetic susceptibility of  $Ba_2[Ni_3N_2]$  as a function of  $T$ .

The crystal structure of  $Ba_2[Ni_3N_2]$  (Fig. 2a) consists of puckered layers  ${}^2_3[Ni_3N_2^{4-}]$  stacked in an AB-sequence. The complex anion  $[Ni_3N_2^{4-}]$  (Fig. 2b) is the first two-dimensional (2D) anion report-

ed for either cobalt, nickel, or copper nitrido-compounds. Nitrogen is coordinated octahedrally by three Ni and three Ba, Ba has a distorted trigonal planar coordination by N, and Ni is linearly coordinated by N. However, it should be noted that the Ni–N bond lengths within the infinite chains are shorter compared to the connecting dumb-bells, but both distances are within the range observed for other nitridonickelates (Fig. 4). Powder X-ray diffraction studies of the low temperature behavior of  $Ba_2[Ni_3N_2]$  (Fig. 2c) show a presumably second order phase transition at  $T \approx 100$  K which affects the intra- and interlayer distances.

Electrical resistivity measurements (Fig. 5) of the solid solution series  $Li_2[(Li_{1-x}Ni_x)N]$  reveal an insulator – metal transition with increasing  $x$  at  $x \approx 0.80$ . Corresponding measurements of the electrical resistivity of barium nitridonickelates show metal-like behavior.  $Ba_2[Ni_3N_2]$  exhibits the lowest resistivity and its crystallographic/magnetic transition at  $T \approx 100$  K is mirrored by a change of the slope of the resistivity at the same temperature.

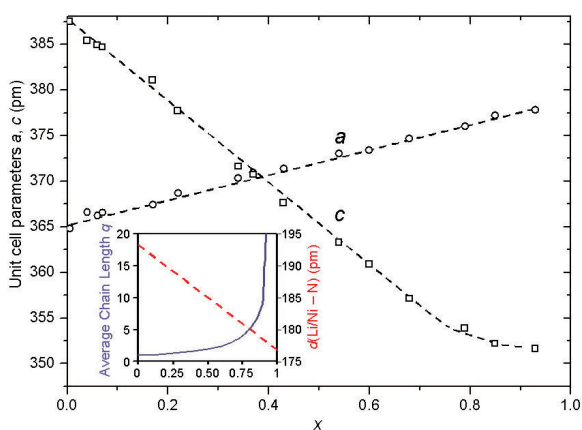


Fig. 3: Hexagonal unit cell parameters  $a$  (circles) and  $c$  (squares) of  $Li_2[(Li_{1-x}Ni_x)N]$  as a function of  $x$ . Dotted lines are guides to the eye.  $d(Li-Ni-N)$  and average chain length  $q$  are shown as inset.

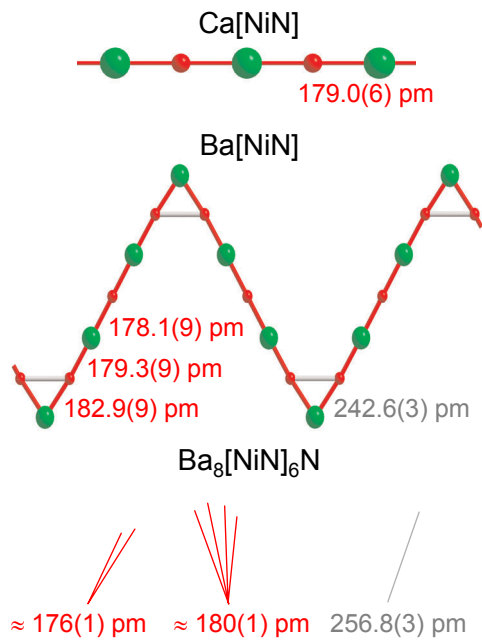


Fig. 4: One dimensional complex anions  ${}_{x}^{1}[\text{NiN}_{2/2}]$  in alkaline-earth nitridonickelates and selected distances  $d(\text{Ni}\cdots\text{Ni})$  and  $d(\text{Ni}-\text{N})$ .

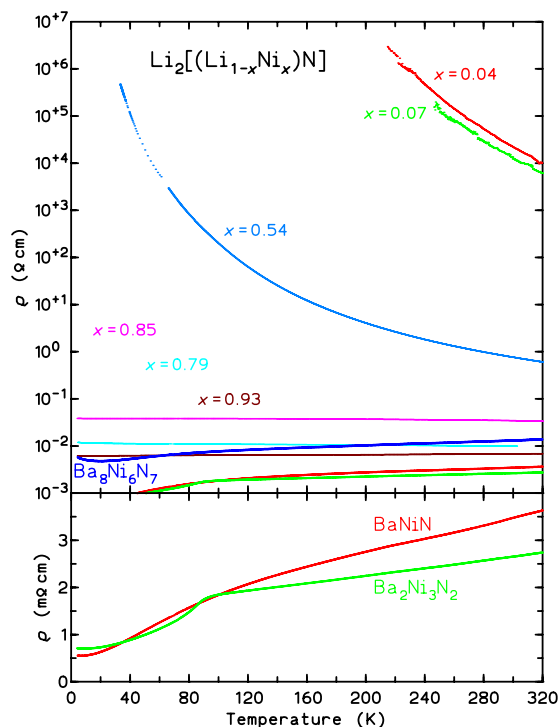


Fig.5: Electrical resistivity of  $\text{Li}_2[(\text{Li}_{1-x}\text{Ni}_x)\text{N}]$ ,  $\text{Ba}[\text{NiN}]$ ,  $\text{Ba}_8[\text{NiN}]_6$ , and  $\text{Ba}_2[\text{Ni}_3\text{N}_2]$  as a function of  $T$  (upper panel: logarithmic scale, lower panel: linear scale).

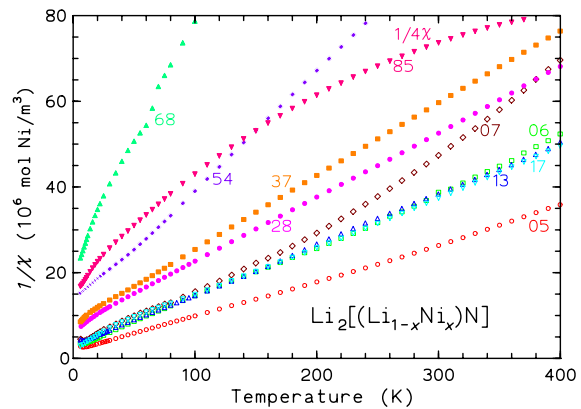


Fig. 6: Inverse magnetic susceptibilities of  $\text{Li}_2[(\text{Li}_{1-x}\text{Ni}_x)\text{N}]$ . Numbers refer to the respective  $x$  values in %. The  $1/\chi$  curve for  $x = 0.85$  is reduced by a factor of four.

The magnetic properties of low-valency nitridonickelates were measured in a wide range of magnetic fields. The inverse magnetic susceptibilities per mole Ni for the substitution series  $\text{Li}_2[(\text{Li}_{1-x}\text{Ni}_x)\text{N}]$  are displayed in Fig. 6. In most cases  $\chi(T)$  obeys a Curie-Weiss law  $\chi(T) = C/(T - \theta)$  above temperatures of 30 K – 50 K. The effective magnetic moments  $\mu_{\text{eff}}/\text{Ni-atom}$  obtained by fitting the experimental data to the above equation are depicted in Fig. 7. They display a strong systematic variation with  $x$ . In samples with small  $x$ ,  $\mu_{\text{eff}}/\text{Ni-atom}$  is large and significantly exceeds the spin-only value for the  $3d^9$  configuration expected for  $\text{Ni}^{+1}$  (dashed level in Fig. 7). For  $x > 0.4$  the effective magnetic moment becomes lower than the respective spin-only value. For intermediate  $x$ ,  $\mu_{\text{eff}}/\text{Ni-atom}$  varies almost linearly with  $x$ . This variation is accompanied by a systematic variation of the Weiss constant  $\theta$ , which is negative and whose absolute value increases with  $x$ . Such strongly negative values of  $\theta$  indicate antiferromagnetic exchange interactions between the  $\text{Ni}^{+1}$  ions, however, no indication of long-range magnetic order was found for any sample. In (hypothetical) samples with  $x = 1$  the nickel species are within infinite Ni–N–Ni chains which are arranged to form hexagonal bundles. The random substitution of the Li(1) sites by Ni-ions in the range of compositions with  $0 < x < 1$  leads to different environments for the magnetic species, interruption of the Ni–N–Ni chains, and to glassy magnetic states at low temperature. For samples with low  $x$  this state might be a spin glass. With increasing  $x$  the antiferromagnetic interactions become stronger but the segmentation of the chains pre-

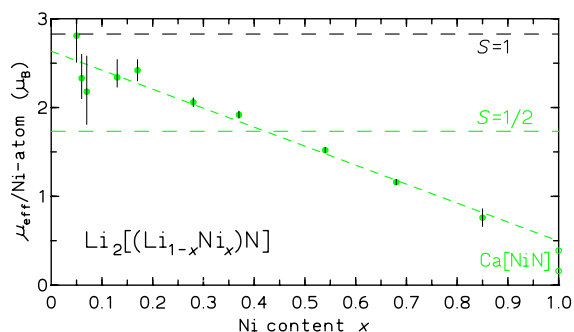


Fig. 7: Effective magnetic moment  $\mu_{\text{eff}}/\text{Ni-atom}$  of samples  $\text{Li}_2[(\text{Li}_{1-x}\text{Ni}_x)\text{N}]$  plotted against the substitution parameter  $x$ . The horizontal levels indicate the spin-only moments expected for  $d^9$  and  $d^8$  states. Open symbols indicate the values reported for  $\text{Ca}[\text{Ni}^{+1}\text{N}]$  [7, 20].

vents the spin system from long-range ordering. For small  $x$  the  $\mu_{\text{eff}}/\text{Ni-atom}$  is significantly larger than the spin-only value and can not be explained completely by the presence of Li(2) vacancies. Assuming a large value  $y(\text{Li}(2)) = 0.01$  of defects implies for  $x = 0.10$  a  $\text{Ni}^{+2}$  concentration of 20 %, which results in only  $\mu_{\text{eff}}/\text{Ni-atom} = 2 \mu_{\text{B}}$  (assuming spin-only values), while the experimental values increase up to  $2.42 \mu_{\text{B}}$ . From observations recently made for the isostructural  $\text{Li}_2[(\text{Li}_{1-x}\text{Fe}_x)\text{N}]$  series (samples with  $x = 0.21$  and  $0.16$ ) [18, 19], it can be suspected that a similar interplay of correlation and orbital effects as in  $\text{Li}_2[(\text{Li}_{1-x}\text{Fe}_x)\text{N}]$  leads to the strong enhancement of  $\mu_{\text{eff}}/\text{Ni-atom}$  for low  $x$  (see “Chemical Bonding Induced Large Magnetic Effects in  $\text{Li}_2[(\text{Li}_{1-x}\text{Fe}_x)\text{N}]$ ”).

On the other hand, the decrease of  $\mu_{\text{eff}}/\text{Ni-atom}$  for  $x > 0.4$  can not be explained by Li(2) defects at all. The magnetism of the hypothetical  $\text{Li}_2[\text{Ni}^{+1}\text{N}]$  might be approximated by the behavior of  $\text{Ca}[\text{Ni}^{+1}\text{N}]$ , which contains similar linear chains  $\infty^1[\text{NiN}_{2/2}^-]$  [7, 8]. These chains are arranged parallel in layers, with the chains in adjacent layers running in perpendicular direction.  $\text{Ca}[\text{NiN}]$  is a metal displaying both Pauli paramagnetism and an electronic term in the heat capacity [7, 20]. The magnetic susceptibility, besides some Ni impurities, follows a modified Curie-Weiss-law  $\chi(T) = \chi_0 + C/(T - \theta)$  [7]. If the resulting  $\mu_{\text{eff}}/\text{Ni-atom} = 0.39 \mu_{\text{B}}$  is considered to be intrinsic, it could be assigned to the segmentation of the chains due to defects within the real crystal structure. Different authors found a value of  $\mu_{\text{eff}}/\text{Ni-atom} = 0.16 \mu_{\text{B}}$  [20]. It can be assumed that an ideal crystal would

have no intrinsic Curie-like paramagnetic contribution. The literature values for  $\mu_{\text{eff}}$  of  $\text{Ca}[\text{Ni}^{+1}\text{N}]$  are included in Fig. 7 and fit well into the trend observed for  $\text{Li}_2[(\text{Li}_{1-x}\text{Ni}_x)\text{N}]$  phases. It may therefore be concluded, that the hypothetical  $\text{Li}_2[\text{Ni}^{+1}\text{N}]$  ( $x = 1$ ) is also a 1D metal and that the systematic variation of  $\mu_{\text{eff}}$  is due to the metal-insulator transition caused by the gradual formation of longer chain segments  $[\text{NiN}_{2/2}^-]_n$  (see inset Fig. 3) and the delocalization of the Ni electronic states with increasing  $x$ .

The magnetic susceptibility of  $\text{Ba}_2[\text{Ni}_3\text{N}_2]$  (Fig. 2d) can be approximated by a Curie-Weiss law only at high temperatures. The effective magnetic moment per formula unit  $\mu_{\text{eff}}/\text{f.u.} = 2.5 \mu_{\text{B}}$  above 150 K is consistent with two  $\text{Ni}^{+1}$  species on the chain-sites and one non-magnetic  $\text{Ni}^0$  species in the “connection-site”, as required by the charge balance, i.e.,  $\text{Ba}_2[\text{Ni}_2^+\text{Ni}^0\text{N}_2]$ . The magnetic system might be therefore a 2D quantum spin ( $S = 1/2$ ) square lattice. Indeed, the rounding of  $\chi(T)$  below  $T \approx 150$  K and the reduction of  $\chi(T)$  below  $T \approx 100$  K is the typical signature of such a 2D quantum spin Heisenberg antiferromagnet on the square lattice. The kink in  $\chi(T)$  at  $T_{\text{N}} = 100$  K and the concomitant strong reduction of the electrical resistivity indicate the long-range antiferromagnetic (Néel) ordering of the  $\text{Ni}^{+1}$  moments. The relatively high  $T_{\text{N}}$  compared to the temperature of the maximum in  $\chi(T)$  indicates a strong out-of-plane exchange coupling. The large spin-disorder scattering contribution in  $\rho(T)$  above  $T_{\text{N}}$  and the coupling to a structural distortion render this compound an interesting magnetic system.

For independent information on the valence states of nickel we employed X-ray absorption spectroscopy (XAS) at the  $K$ -threshold of Ni. Figure 8a shows NiK XAS spectra of phases  $\text{Li}_2[(\text{Li}_{1-x}\text{Ni}_x)\text{N}]$  with different  $x$ , together with spectra of Ni and  $\text{Ni}^{+2}\text{O}$  as references. The spectra exhibit an enhanced pre-edge feature around 8337 eV due to breaking of the local centro-symmetry at Ni by Li-Ni-disorder within the lateral environment. This enhanced  $1s \rightarrow 3d$  transition lies close to the main edge jump  $1s \rightarrow 4p$  above 8345 eV (only observed as a shoulder), thus the inflection point of the main absorption edge and the pre-edge peak can not be determined independently. The edge energies of the substitution phases are much closer to those of Ni than to the  $\text{Ni}^{+2}$ -reference compounds. Comparing different compo-

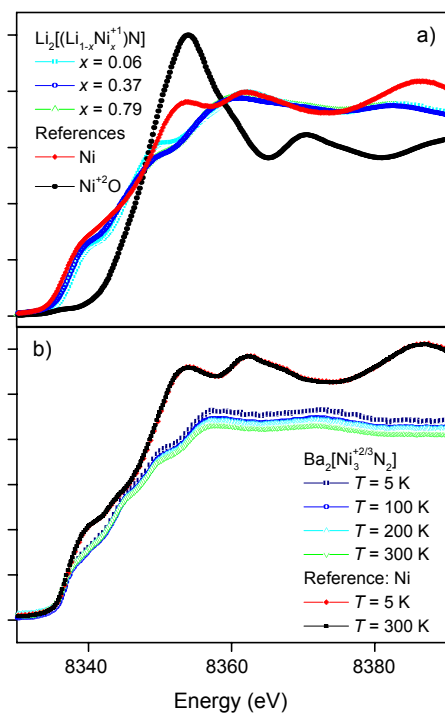


Fig. 8: XAS spectra at the NiK edge of phases a)  $\text{Li}_2[(\text{Li}_{1-x}\text{Ni}_x)\text{N}]$  at 298 K, b)  $\text{Ba}_2[\text{Ni}_3\text{N}_2]$  at different temperatures. Reference compounds were added for comparison.

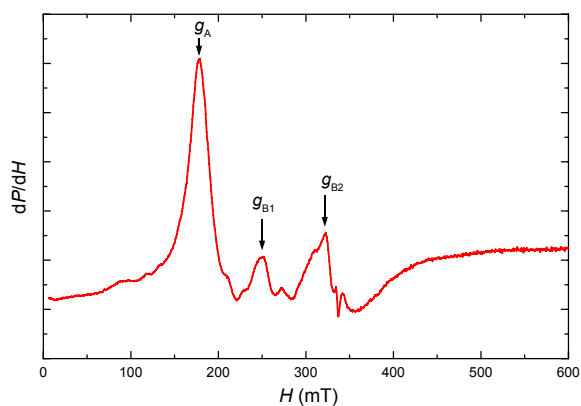


Fig. 9: ESR spectrum of  $\text{Li}_2[(\text{Li}_{1-x}\text{Ni}_x)\text{N}]$  ( $x = 0.04$ ) at  $T = 4.2$  K.

sitions, the main structure gains intensity due to  $4p$   $e^-$  charge reduction and the pre-edge peak loses intensity, i.e., less  $1s \rightarrow 3d$  transition occurs in the spectrum for the phase with the lowest  $x$ . This corresponds to a larger proportion of Ni in a highly symmetric surrounding with six Li-neighbors within the lateral plane in the phases with small  $x$  (in other words, a smaller degree of  $4p/3d$  mixing) in agreement with the statistical distribution of Ni over the Li(1) positions from the structural model. But altogether, the difference in the intensities of the pre-edge features for different compositions are hardly visible, indicating only a small shift of the pre-edge peak and the main absorption to higher energies with respect to Ni metal. Still, the results indicate an average oxidation state of Ni for the whole  $\text{Li}_2[(\text{Li}_{1-x}\text{Ni}_x)\text{N}]$  series only slightly above +1, most likely compensated within the crystal structure by Li-vacancies. ESR measurements confirmed the +1 oxidation state of the Ni ion; the ESR spectrum of  $\text{Li}_2[(\text{Li}_{1-x}\text{Ni}_x)\text{N}]$  ( $x = 0.04$ ) at  $T = 4.2$  K (Fig. 9) is represented by a very intensive line with  $g_A \approx 3.8$  and two other weaker signals  $g_{B1} \approx 2.68$  and  $g_{B2} \approx 2.08$ . These three lines correspond to  $\text{Ni}^{+1}$  ions [21], which are located within three different lateral environments built up by six Li/Ni positions.

The XAS spectra of  $\text{Ba}_2[\text{Ni}_3\text{N}_2]$  for different temperatures are shown in Fig. 8b. Due to the non-centrosymmetrical local symmetry of Ni and the two crystallographic independent Ni atoms in this structure, the spectra show several transitions close in energy. The four prominent steps become slightly more pronounced with decreasing temperature, but remain at a constant energy level. A detailed investigation of this observation is currently underway.

\* Current address: Institut für Anorganische Chemie, Christian-Albrechts-Universität zu Kiel, Olshausenstr. 40, 24098 Kiel, Germany

\*\* II. Physikalisches Institut der Universität zu Köln, Zùlpicher Str. 77, 50937 Köln, Germany

## References

- [1] W. Burow, J. Birx, F. Bernhardt, R. Hoppe, *Z. Anorg. Allg. Chem.* **619**, 923 (1993).
- [2] R. Kniep, *Pure & Appl. Chem.* **69**, 185 (1997).
- [3] R. Niewa, F. J. DiSalvo, *Chem. Mater.* **10**, 3733 (1998).
- [4] A. Rabenau, H. Schulz, *J. Less-Common Met.* **50**, 155 (1976).
- [5] W. Sachsze, R. Juza, *Z. Anorg. Allg. Chem.* **259**, 278 (1949).
- [6] R. Niewa, F. R. Wagner, W. Schnelle, O. Hochrein, R. Kniep, *Inorg. Chem.* **40**, 5215 (2001).
- [7] M. Y. Chern, F. J. DiSalvo, *J. Solid State Chem.* **88**, 459 (1990).
- [8] A. Gudat, R. Kniep, J. Maier, *J. Alloys Comp.* **186**, 339 (1992).
- [9] A. Gudat, R. Kniep, A. Rabenau, *Thermochim. Acta* **160**, 49 (1990).
- [10] A. Gudat, S. Haag, R. Kniep, A. Rabenau, *J. Less-Comm. Met.* **159**, 29 (1990).
- [11] A. Gudat, W. Milius, S. Haag, R. Kniep, A. Rabenau, *J. Less-Comm. Met.* **168**, 305 (1991).
- [12] A. Mehta, P. Höhn, R. Kniep, *Z. Anorg. Allg. Chem.* **628**, 2173 (2002).
- [13] A. Gudat, PhD Thesis, Universität Düsseldorf 1990.
- [14] M. G. Barker, A. J. Blake, P. P. Edwards, D. H. Gregory, T. A. Hamor, D. J. Siddons, S. E. Smith, *Chem. Commun.* **13**, 1187 (1999).
- [15] J. Klatyk, P. Höhn, R. Kniep, *Z. Kristallogr. NCS* **213**, 31 (1998).
- [16] M. T. Weller, S. E. Dann, P. F. Henry, D. B. Currie, *J. Mater. Chem.* **9**, 283 (1999).
- [17] D. H. Gregory, P. M. O'Meara, A. G. Gordon, J. P. Hodges, S. Short, J. D. Jorgensen, *Chem. Mater.* **14**, 2063 (2002).
- [18] J. Klatyk, W. Schnelle, F. R. Wagner, R. Niewa, P. Nowák, R. Kniep, M. Waldeck, V. Ksenofontov, P. Gütlich, *Phys. Rev. Lett.* **88**, 207202 (2002).
- [19] J. Klatyk, R. Niewa, F. R. Wagner, W. Schnelle, Z.-L. Huang, H. Borrmann, R. Kniep, Scientific Report 2000, 116, "Low-valency Nitridometallates" MPI CPfS, Dresden, Germany.
- [20] S. Shamoto, T. Kato, K. Ohoyama, M. Ohashi, Y. Yamaguchi, T. Kajitani, *J. Phys. Chem. Solids* **60**, 1157 (1999).
- [21] S. A. Altshuler, B. M. Kosyrev, *Electron Paramagnetic Resonance in Compounds of Transition Metals*, Wiley, New York, 1975.